EARTH SURFACE PROCESSES AND LANDFORMS
Earth Surf. Process. Landforms **41**, 791–808 (2016)

Published online 28 December 2015 in Wiley Online Library
(wileyonlinelibrary.com) DOI: 10.1002/esp.3864

Distinct patterns of interaction between vegetation and morphodynamics

Mijke van Oorschot,[1,2]* Maarten Kleinhans,[1] Gertjan Geerling[2] and Hans Middelkoop[1]
[1] Faculty of Geosciences, Universiteit Utrecht, 3508 TC Utrecht, The Netherlands
[2] Deltares, Department of Freshwater Ecology & Water Quality, 2600 MH Delft, The Netherlands

Received 16 July 2015; Revised 29 October 2015; Accepted 4 November 2015

*Correspondence to: Mijke van Oorschot, Faculty of Geosciences, Universiteit Utrecht, 3508 TC Utrecht, The Netherlands. E-mail: mijke.vanoorschot@deltares.nl

ESPL
Earth Surface Processes and Landforms

ABSTRACT: Dynamic interaction between river morphodynamics and vegetation affects river channel patterns and populations of riparian species. A range of numerical models exists to investigate the interaction between vegetation and morphodynamics. However, many of these models oversimplify either the morphodynamics or the vegetation dynamics, which hampers the development of predictive models for river management. We have developed a model coupling advanced morphodynamics and dynamic vegetation, which is innovative because it includes dynamic ecological processes and progressing vegetation characteristics as opposed to commonly used static vegetation without growth and mortality. Our objective is to understand and quantify the effects of vegetation-type dependent settling, growth and mortality on the river pattern and morphodynamics of a meandering river. We compared several dynamic vegetation scenarios with different functional trait sets to reference scenarios without vegetation and with static vegetation without growth and mortality. We find distinct differences in morphodynamics and river morphology. The default dynamic vegetation scenario, based on two Salicaceae species, shows an active meandering behaviour, while the static vegetation scenario develops into a static, vegetation-dominated state. The diverse vegetation patterns in the dynamic scenario reduce lateral migration, increase meander migration rate and create a smoother floodplain compared to the static scenario. Dynamic vegetation results in typical vegetation patterns, vegetation age distribution and river patterns as observed in the field. We show a quantitative interaction between vegetation and morphodynamics, where increasing vegetation cover decreases sediment transport rates. Furthermore, differences in vegetation colonization, density and survival create distinct patterns in river morphology, showing that vegetation properties and dynamics drive the formation of different river morphologies. Our model demonstrates the high sensitivity of channel morphodynamics to various species traits, an understanding which is required for floodplain and stream restoration and more realistic modelling of long-term river development. Copyright © 2015 John Wiley & Sons, Ltd.

KEYWORDS: biogeomorphology; river morphodynamics; river meandering; vegetation patterns; dynamic riparian vegetation model

Introduction

Riparian vegetation interacts with morphological processes to create distinct habitat mosaics (for reviews, see Tockner and Stanford, 2002; Gurnell, 2014) and river patterns (for reviews, see Bertoldi *et al.*, 2009; Kleinhans, 2010). Although numerous studies have described the links between biological and physical characteristics in rivers (e.g. Bertoldi *et al.*, 2009; Corenblit *et al.*, 2011; Gurnell, 2014), these are mainly empirical and the underlying processes are known only in outline. Currently, there is insufficient quantitative understanding of the dynamic interactions in these systems to integrate this knowledge in predictive models for river management (Vaughan *et al.*, 2009).

Riparian vegetation both affects and is affected by morphodynamic processes. Vegetation can increase the strength of river banks by reinforcing the soil by root development and by increasing soil cohesion through the addition of organic material (Simon and Collison, 2002). Conversely, vegetation can also decrease bank stability by affecting the hydrological regime in the bank, which can cause mass failure (Rinaldi and Casagli, 1999). Vegetation can alter the flow field and subsequently the sediment balance through hydraulic resistance, which is determined by parameters such as plant density, plant thickness, plant height and flexibility (Järvelä, 2002; Baptist *et al.*, 2007; Zong and Nepf, 2011). This means that the degree to which vegetation is affected by morphodynamics depends on the characteristics of the vegetation. Riparian vegetation has specialized in withstanding dynamic conditions by developing life history strategies with traits enabling them to survive periods of flooding, scour, burial and high flow velocities (Karrenberg *et al.*, 2002). These species have also adapted their timing and period of seed dispersal to the flow regime (Van Splunder *et al.*, 1995; Greet *et al.*, 2011). For instance, several Salicaceae species such as willows and cottonwoods have different seed dispersal windows, resulting in a vegetation zonation at different elevations on river bars and banks (Van Splunder *et al.*, 1995). In turn, such species act as ecosystem engineers because they colonize and subsequently stabilize the location where they grow, as well as demobilize bare substrate around the vegetation patch (Corenblit *et al.*, 2009). This hydraulic resistance can lead, on the one hand, to flow diversion into the river channel (Luhar *et al.*, 2008) and, on the other hand, to deposition of fine sediment and

organic material within and behind the vegetation patch (Zong and Nepf, 2011). The interplay between vegetation and morphodynamics creates habitat variation in terms of elevations, substrate, flow conditions and nutrient availability, which form new niches for other species and is therefore the first step in the chain of vegetation succession (Gurnell, 2014).

Meandering rivers are formed by the interplay between erosion of the outer bend and deposition on the point bars in the inner bend (Roberts, 2003). Highly sinuous rivers are formed when the point bars are stabilized, i.e. by vegetation development, thereby preventing chute cut-offs and promoting lateral expansion of the meander bends (Schuurman *et al.*, 2015). But the extent of vegetation stabilization and thereby the formation of river floodplain strongly depends on the type of vegetation. Therefore one would expect that vegetation properties and dynamics play a large role in shaping the river planform.

There are many modelling studies describing the effect of morphodynamics on vegetation by predicting vegetation distribution and succession depending on morphodynamic parameters such as flooding duration and shear stress (Camporeale and Ridolfi, 2010; Rivaes *et al.*, 2014; García-Arias and Francés, 2015), or solely focusing on the effects of vegetation on flow resistance (Aberle and Järvelä, 2013; Luhar and Nepf, 2013) or mechanical bank dynamics (Pollen-Bankhead and Simon, 2010). Furthermore, there are analytical modelling studies including the two-way interaction between vegetation and morphodynamics that show the effect of vegetation biomass on meander migration dynamics (Perucca *et al.*, 2007) and landscape topography (Vesipa *et al.*, 2015).

Experimental research has shown that uniform vegetation development in floodplains can transform rivers from multi-thread to single-thread channels (Braudrick *et al.*, 2009; Tal and Paola, 2010; Van Dijk *et al.*, 2013). Likewise, numerical modelling with cellular automata (Murray and Paola, 2003; Coulthard *et al.*, 2007) and higher-complexity, physics-based modelling studies (Crosato and Saleh, 2011; Nicholas, 2013; Bertoldi *et al.*, 2014) suggest such pattern-transforming effects by vegetation in rivers. However, most numerical models to date are hampered by oversimplification of either the morphodynamics or the vegetation dynamics (Solari *et al.*, 2015). Most studies with cellular automata included more ecological processes, such as colonization, growth, resource utilization and mortality, than studies conducted with physics-based models. However, the morphodynamic processes in cellular automata are rather simplistic as they do not reproduce grid-independent bar dimensions found in nature and predicted by theory (Schuurman *et al.*, 2013). The results are mainly qualitative and cannot handle situations with large parameter fluctuations (Coulthard *et al.*, 2007). More complex models include phenomena on longer length scales, such as backwater effects, and detailed transverse slope effects on sediment transport that are essential to reproduce bar patterns (Schuurman *et al.*, 2013). In such advanced physics-based models, however, vegetation is often simplified to uniformly distributed, static cylinders without growth or mortality. None of the advanced physics-based modelling studies discussed above have implemented these dynamic vegetation properties in their models. This results in a predefined dense, static effect of vegetation on river morphology as opposed to a heterogeneous natural vegetation cover which is actively interacting with morphodynamics. However, to be able to predict long-term river and floodplain evolution and coexisting vegetation, it is necessary to link dynamic ecological processes to advanced morphodynamics (Stella *et al.*, 2006; Camporeale *et al.*, 2013; Curran and Hession, 2013).

Our objective is to understand and quantify effects of vegetation-type dependent settling, growth and mortality with life-stage dependent hydraulic resistance on the river pattern and morphodynamics of a meandering river. To this end we present a model coupling hydraulic resistance caused by multiple vegetation types, depending on seed dispersal, colonization, growth and mortality, to a two-dimensional model that solves unsteady flow, sediment transport and morphological change at the spatial and temporal resolution appropriate for river channel–floodplain interactions. We compare river planform, vegetation pattern and morphodynamics for a scenario containing vegetation with dynamic properties based on two Salicaceae species to reference scenarios without vegetation and with commonly used static vegetation. Furthermore, we quantitatively analyse the interaction between vegetation and morphodynamics and test the applicability of the model by evaluating several vegetation types with different properties and sensitivities for morphodynamic pressures.

Methods

Morphodynamic model description

We modelled morphodynamics with the Delft3D code (version 4.00.01) for a river reach with about three meander wavelengths and we developed a new model for vegetation dynamics which we coupled to Delft3D. Delft3D was chosen because it is one of the most comprehensive scientific morphodynamic models to date that has been successfully applied and validated in a large number of scientific studies (e.g. Langendoen, 2001; Lesser *et al.*, 2004; Gerritsen *et al.*, 2007) and engineering studies where accuracy of the order of decimetres is important (see Schuurman *et al.*, 2013, for examples). Here we use the two-dimensional, depth-averaged flow option for reasons of efficiency, and we calculate sediment transport and bed-level changes (see Schuurman *et al.*, 2013, for details on parameters and settings). The hydrodynamic and morphodynamic time steps were chosen to attain feasible calculation times for the required resolution and were set to respectively 0.2 and 6 min. A constant morphological multiplication factor of 30 was applied to the bed-level changes per hydrodynamic time step. The total run time of the model was 300 years. Detailed parameter settings can be found in Table I. Hydraulic resistance caused by vegetation was calculated in each grid cell for flow through vegetation and flow above vegetation from the Baptist *et al.* (2007) relation:

$$C = \frac{1}{\sqrt{\frac{1}{C_b^2} + \frac{C_d n h_v}{2 \cdot g}}} + \frac{\sqrt{g}}{\kappa} \ln \frac{h}{h_v} \tag{1}$$

where C is the Chezy value of the vegetation ($m^{\frac{1}{2}}/s$), C_b is the Chezy value for the unvegetated parts, c_d is the drag coefficient, n is vegetation density (stem diameter × number of stems per m^2), h_v is the height of the vegetation (m), h is water depth (m), κ is the Von Karman constant (0.41) and g is gravitational force (9.81 m/s^2). Multiple vegetation types, here we use two, with different ages and different properties can occur in one grid cell, so the Chezy value was calculated separately for each type and age, and subsequently the total sequential Chezy coefficient was calculated weighted by fraction coverage.

Vegetation model description

We modelled vegetation in Matlab (R2013b) by retrieving bed levels, flow velocities and water levels from Delft3D at the beginning of each ecological time step and restarting it

Table I. Morphodynamic parameter settings

Parameter	Value	Unit	Reference or motivation
Timespan model run	300	yr	At least one life cycle of a riparian tree
Hydrodynamic timestep	0.2	min	Based on grid cell size and flow velocity
Morphological scale factor	30	—	Schuurman *et al.* (2013)
Timestep bed-level change	6	min	
Timestep vegetation	21 900	min	To capture main ecological processes
Grid size (width × length)	1000 × 3600	m	Covering a few meanders
Cell size (width × length)	25 × 25	m	Compromise between resolution and model efficiency
Chezy value bare substrate	25	$m^{\frac{1}{2}}/s$	Van Dijk *et al.* (2014)
*D*50	5×10^{-3}	m	Van Dijk *et al.* (2014)
Sediment transport predictor	Engelund–Hansen	—	Schuurman *et al.* (2013)
Initial sinuosity	1.3870	—	Geerling *et al.* (2006)

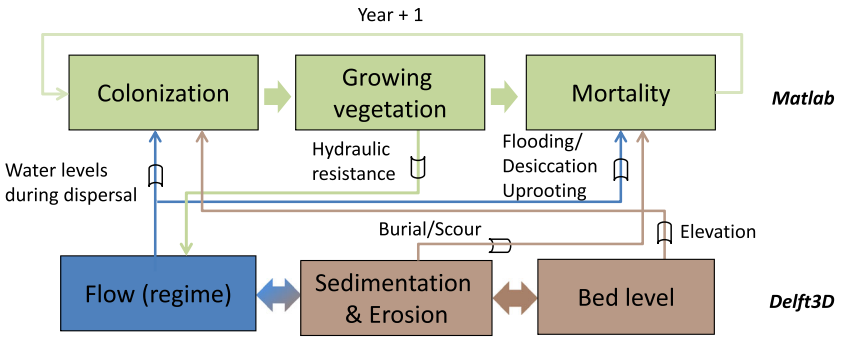

Figure 1. Flow diagram of processes and dynamic interactions in the model. This figure is available in colour online at wileyonlinelibrary.com/journal/espl

with updated information on vegetation characteristics that were used in Delft3D for hydraulic resistance calculations (Figure 1). Riparian trees (Salicaceae species) were selected as the main vegetation types because these are the dominant ecosystem engineering species that grow on river floodplains in northwestern Europe (Corenblit *et al.*, 2009; Gurnell, 2014). The ecological time step was set to approximately 2 weeks to maintain an adequate interval for ecological processes, leading to 24 time steps within 1 year. At the beginning of each ecological time step, the morphodynamic model was paused, vegetation processes were calculated and updated vegetation location and characteristics were fed back into the morphodynamic model. All vegetation processes were handled within 1 year. The general vegetation processes are explained below.

We specified two vegetation types with general characteristics and life stage-specific parameters. General characteristics are maximum age, initial sizes of shoot, root and stem diameter (for seedlings), growth factors for logarithmic growth of shoot, root and stem diameter and timing of seed dispersal. Life stage-specific parameters are the number of stems per unit area, the fraction of area covered per grid cell, a drag coefficient, and mortality rules for flooding, desiccation and uprooting due to high flow velocity. This means that we could account for changing characteristics such as plant shape, which is relevant for interaction with morphodynamics, throughout the life cycle of a vegetation type.

Colonization of riparian tree seedlings takes place on moist, bare substrate between the maximum and minimum water levels during the dispersal window, i.e. the time period of successful germination of a species. This colonization mechanism was also described in Corenblit *et al.* (2009) and Gurnell (2014). Many riparian pioneer tree species also employ asexual reproduction as a means of dispersal (Karrenberg *et al.*, 2002). However, in our study area along the River Allier, most adult vegetation stands of *Populus nigra* originated from seeds, confirming our choice for only taking sexual reproduction into account (Legionnet *et al.*, 1997). Following the dispersal window, vegetation was assigned to the grid cells. We assumed that seed supply was unlimited, causing seedlings to fill all grid cells within the boundaries of the bare substrate. This is a valid assumption for dominant riparian trees with a large seed production (Braatne *et al.*, 1996). Seedlings were allowed to settle in grid cells with a density depending on the degree of antecedent vegetation cover as follows: if a colonized grid cell was empty, the grid cell was assigned a fraction of the colonizing vegetation type according to the predefined initial cover fraction. A cover fraction of 1 represents a completely filled grid cell. If a cell was partially covered by other vegetation, the cell was filled up with seedlings up to a fraction of one. This means that multiple vegetation types with different ages can reside in a single grid cell and there is competition for space.

Vegetation growth of shoot, root and stem diameter were implemented as logarithmic growth functions as a result of age calculated with the following formula:

$$G = F_v \log(a) \tag{2}$$

where G is the size (i.e. of the shoot, root or stem diameter) in meters, F_v is the vegetation-type dependent logarithmic growth factor and a is the vegetation age in years. The size of the seedlings was taken from the initial conditions of the first life stage. When vegetation survived the calendar year, it increased in age until the maximum age was reached.

Mortality of vegetation is calculated at the end of each calendar year and depends on days of subsequent flooding per year, days of subsequent desiccation per year, maximum flow velocities, burial and scour. Subsequent days of flooding or desiccation were recorded by registering wet and dry cells at average water levels within two ecological time steps. If a cell did not change from wet to dry or vice versa between

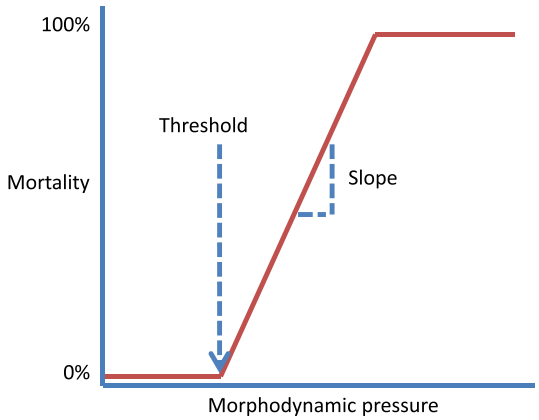

Figure 2. Example of the dose–effect relation between vegetation mortality and morphodynamic pressure. Morphodynamic pressures are duration of flooding or desiccation (in days) or flow velocity (m/s). The threshold determines the onset of vegetation mortality and the slope determines the range of conditions over which mortality increases. A vertical slope means a sharp threshold. Thresholds and slopes are specified as input for the three morphodynamic pressures for all life stages of all vegetation types. This figure is available in colour online at wileyonlinelibrary.com/journal/espl

ecological time steps, it was recorded and added to the value already present in the matrix. At the end of the year, the wetting and drying matrices were multiplied by the number of ecological time steps within that year.

Mortality by flooding, desiccation and high flow velocities was determined by a dose–effect relation, where the percentage of plants not surviving the morphodynamic pressure was on the *y*-axis and the morphodynamic pressure was on the *x*-axis (Figure 2). The relation contains a threshold value after which the vegetation started to die, and a mortality fraction of the vegetation related to the pressure, which was determined by the slope of the curve. The slope was implemented as a value between 0 and 1, where 1 is a vertical line representing immediate mortality after the threshold is exceeded and 0 is a horizontal line representing no mortality. The threshold and the slope were user defined and were set for each life stage per vegetation type. Mortality was implemented by reducing the fraction of the corresponding vegetation type within a grid cell. This was done by calculating the mortality percentage from the mortality curve as a portion of the initial fraction (mortality fraction = mortality × initial fraction), which was then subsequently subtracted from the current fraction before mortality (new fraction = current fraction − mortality fraction). In this way the cell could become completely empty and no small fractions would remain if the mortality percentage did not reach 100% in time. Vegetation dies through burial if the whole plant was buried. This is the case if the amount of sedimentation was higher than the plant shoot height. Vegetation dies through scour if the scour depth exceeds the plant root length. Sedimentation and erosion are calculated as bed-level differences between two ecological time steps, where the maximum value in all ecological time steps is stored per year and subsequently used to calculate burial and scour. When the maximum vegetation age is reached, vegetation dies due to senescence.

Model set-up

Model parametrization, initial and boundary conditions were loosely based on a reach of the River Allier in France (Figure 3). The River Allier is a rain-fed, gravel-bed river originating from the Massif Central, with a mean annual flood discharge of 500 m^3/s and mean annual minimum discharge of 27 m^3/s (Crosato and Saleh, 2011; Van Dijk *et al.*, 2014). The Allier is one of the main tributaries of the River Loire. Part of the river valley is a designated natural reserve area without navigation and flow regulation where the river follows a meandering planform (Geerling *et al.*, 2006). The Allier is highly dynamic, with active growth of point bars, erosion of outer banks and frequent chute cut-offs (Kleinhans and van den Berg, 2011). The riparian vegetation consists of pioneer trees, herbaceous vegetation, softwood forest, hardwood forest, shrubs and grass. The vegetation cover is changing dynamically related to changes in the fluvial morphology (Geerling *et al.*, 2006). This dynamic interaction is the most interesting for our purpose to critically test our model concept – more interesting than cases where either the morphodynamics or the vegetation is dictating the dynamics.

Boundary and initial conditions were applied as follows. The upstream discharge was sampled from five generalized discharge years of the Allier and ranging from 400 m^3/s in winter to 50 m^3/s in summer (Figure 4C). Downstream water levels related to discharge were determined iteratively by hydrodynamic modelling for static bed levels in the absence of vegetation. The initial bed level (Figure 4A) featured about three wavelengths of regular meander bends, because the aim of our study was to investigate effects of vegetation on meandering but not the onset of meandering from an initially straight channel. The latter would have taken a considerably longer model time and perhaps processes of floodplain formation by cohesive sediment which are presently not included. Meander length was based on general channel dimensions of the River Allier extracted from aerial photos and bar length theory (Struiksma, 1986; Kleinhans and van den Berg, 2011) and values reported in the literature (Geerling *et al.*, 2006; Crosato and Saleh, 2011). Uniform sediment with $D50 = 5$ mm was used, representing fine gravel. Sediment transport was calculated in Delft3D using the transport predictor of Engelund–Hansen with transverse bed slope settings as in Schuurman *et al.* (2013). For the initial conditions this resulted for high and low flow respectively in typical water depths in the channel of 3 and 1.2 m, flow velocities of 1 and 0.6 m/s, channel widths of about 200 and 75 m and Shield numbers

Figure 3. Location of the study site: a meandering reach of the River Allier in France. This figure is available in colour online at wileyonlinelibrary.com/journal/espl

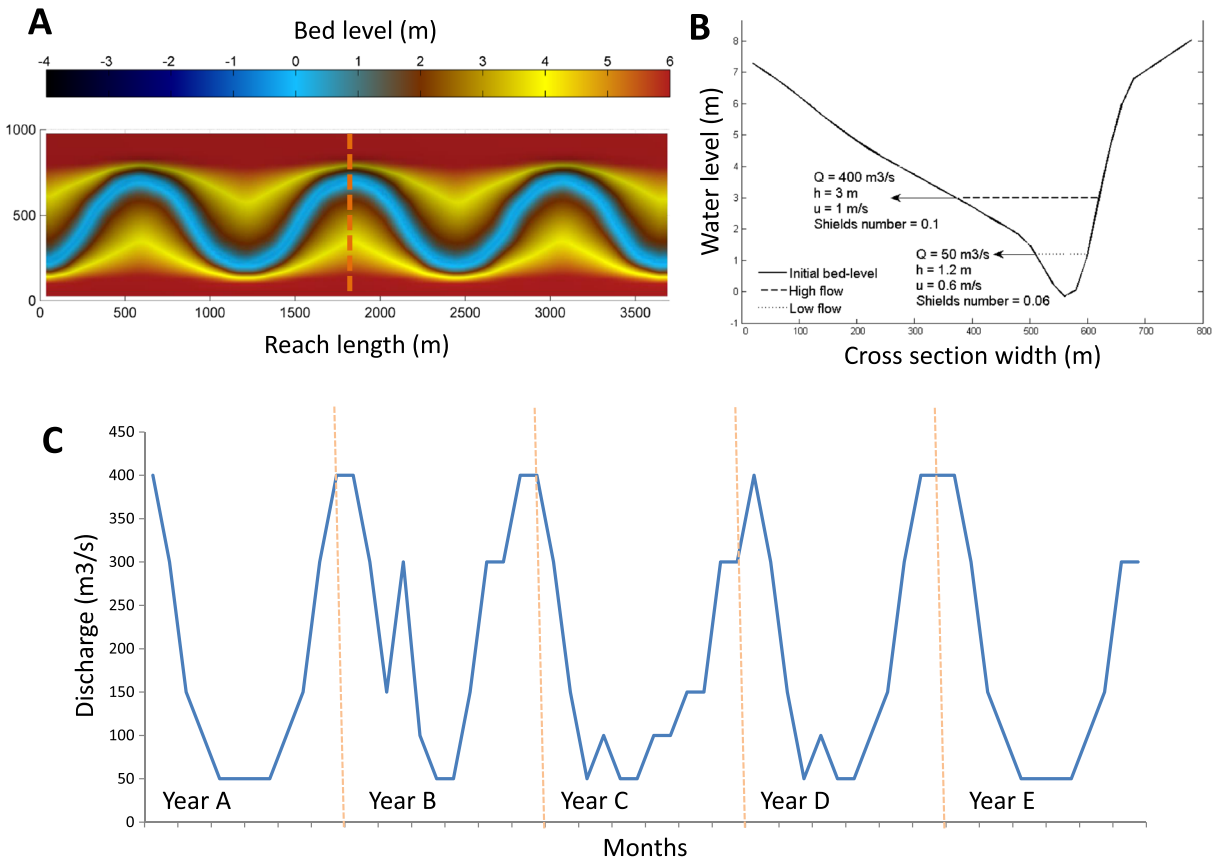

Figure 4. Initial conditions and boundary conditions for the model. (A) Initial bed level detrended with valley gradient. Dashed line is the location of the cross-section in (B) with maximum and minimum water levels in the initial conditions. (C) Five time series of flow discharge over 1 year, randomly selected for a time series of 300 years. This figure is available in colour online at wileyonlinelibrary.com/journal/espl

of 0.1 and 0.06 (Figure 4B). Lateral channel erosion due to bank failure processes was ignored in the present model, as this requires a much higher grid resolution near the banks, a deforming curvilinear grid or an immersed boundary (Van Dijk *et al.*, 2014; Schuurman *et al.*, 2015). Migration of the meander bends in our model takes place when the banks are submerged, as caused by the transverse bed slope effect, and when erosion takes place. Adjacent dry cells are also reduced in height to simulate bank failure but this is only relevant at the valley walls in the model. This study focuses on sustained meandering due to dynamic vegetation rather than initiation of meandering from a straight channel, where bank erosion processes would be more important. In our case the processes on the point-bar are most relevant.

We ran our default dynamic vegetation model and two control runs: one without vegetation but otherwise the same conditions (Table I), and one with static vegetation as commonly used until now. The main difference between the static and dynamic scenarios is that in the static scenario vegetation is uniformly distributed across the floodplain each year and does not grow or die, whereas the dynamic scenario explicitly considers changing spatial distribution and vegetation characteristics associated with colonization, ageing and mortality. The static vegetation scenario represents the way vegetation has been modelled until now, while the dynamic method is an innovative and more realistic way of vegetation representation. In the dynamic scenario we parametrized two Salicaceae type species that are typical for rivers in northwestern Europe (Table II), namely a *Salix* type and a *Populus* type, which differ in seed dispersal timing, maximum age and mortality tolerances for flooding and desiccation. *Salix* disperses its seeds in June, has a maximum age of 60 years and is more tolerant to flooding. *Populus* disperses its seeds in May, has a maximum age of 150 years and is more tolerant to desiccation. In the static vegetation scenario, vegetation colonized in dry cells each year with a dispersal timing set between *Salix* and *Populus* and did not grow or die. The static interaction parameters for shoot length, stem diameter and number of stems/m^2 are set to a 10-year-old bush averaged for *Salix* and *Populus*. The mortality limits for both vegetation types were initially parametrized to broadly fit the age distribution of pioneer, bush and forest vegetation deduced by Geerling *et al.* (2006) after 10 years and fall within occurrence ranges for softwood forests reported in the literature (Van Velzen *et al.*, 2003a).

Data analysis

To characterize the patterns and dynamics in morphology and vegetation, we analysed the model output of each scenario as follows. All bed-level data were detrended by the valley gradient, so that the cross-sectionally averaged bed level was zero for the entire reach. Immediate boundary effects were excluded by clipping 500 m (20 grid cells) off the upstream and downstream boundaries. We then calculated bed-level distributions for the entire clipped grid and determined median, 5% and 95% bed elevations to plot as time series. To compare hydraulic resistance effects of morphology and vegetation, water levels were calculated each year as the maximum in a cross-section in the middle of the reach.

Sinuosity was calculated per year as the length of the path of cross-sectional maximum flow velocity divided by the length of the valley. Flow velocity values with large coordinate jumps,

Table II. General vegetation parameter settings of *Salix* and *Populus* and for four different life stages. LS1, seedlings; LS2, bush; LS3, forest; LS4, degeneration. Seedlings are small and susceptible to morphodynamic pressures, stakes form the bush phase with dense patches, forest is older and less dense and degeneration represents dead or dying trees

Parameter	Unit	Vegetation type 1	Vegetation type 2	Reference
Vegetation type	—	*Salix* type	*Populus* type	Main riparian ecosystem engineers, Gurnell (2014)
Maximum age	yr	60	150	Braatne *et al.* (1996); Peters (2002)
Initial root length	m	0.1	0.5	Canadell *et al.* (1996)[a]
Initial shoot length	m	0.25	0.1	Van Velzen *et al.* (2003b)
Initial stem diameter	m	0.002	0.036	Van Velzen *et al.* (2003b)
Logarithmic growth factor root (F_v Equation (2))	—	0.85	1.15	Canadell *et al.* (1996)[a,b]
Logarithmic growth factor shoot (F_v Equation (2))	—	11.5	14	Kleyer *et al.* (2008)[a]
Logarithmic growth factor stem diameter (F_v Equation (2))	—	0.41	0.6	Van Velzen *et al.* (2003b)[a]
Timing of seed dispersal	month	6 (June)	5 (May)	Kleyer *et al.* (2008); Van Splunder *et al.* (1995)

Parameter		Life stages *Salix* type				Life stages *Populus* type				
	Unit	LS1	LS2	LS3	LS4	LS1	LS2	LS3	LS4	Reference
Number of years in life stage	yr	1	9	40	10	1	9	130	10	Adapted from Van Velzen *et al.* (2003b)
Number of stems	stems/m^2	25	15	0.16	0.16	25	13	0.27	0.27	Van Velzen *et al.* (2003b); Wolf *et al.* (2001)
Area fraction (0–1)	—	0.8	0.8	0.8	0.8	0.8	0.8	0.8	0.8	Initial guess
Drag coefficient	—	1	1.5	1.5	1.5	1	1.5	1.5	1.5	Van Velzen *et al.* (2003b); Fotherby *et al.* (2012)
Desiccation threshold	days	25	190	240	365	35	210	260	365	Geerling *et al.* (2006)[c]
Desiccation slope	—	0.75	0.3	0.3	1.0	0.75	0.3	0.3	1.0	Geerling *et al.* (2006)[c]
Flooding threshold	days	70	260	310	365	60	240	290	365	Geerling *et al.* (2006)[c]
Flooding slope	—	0.75	0.3	0.3	1.0	0.75	0.3	0.3	1.0	Geerling *et al.* (2006)[c]
Flow velocity threshold	m/s	0.55	7.0	12.0	6.0	0 .55	7.0	12.0	6.0	Geerling *et al.* (2006)[c]
Flow velocity slope	—	0.75	0.3	0.3	0.3	0.75	0.3	0.3	0.9	Geerling *et al.* (2006)[c]

[a] Value extracted from the logarithmic growth curve created to fit the maximum parameter value found in the literature.
[b] Fact sheet from Istituto di Biologia Agroambientale e Forestale (http://www.ibaf.cnr.it/en/, consulted in 2014).
[c] Age distribution in Geerling *et al.* (2006) used for mortality thresholds and slope determined after 10-year run.

caused by chute bars temporarily having a higher flow velocity than the main channel, were filtered out. This was done by calculating the absolute difference between the *y*-coordinates of two subsequent flow velocity values and deleting all values that exceeded four grid cells, i.e. approximately one channel width. The flow path was smoothed by a moving average over three grid cells. Meander migration rate was calculated as the average minimal shift of the flow path as calculated for the sinuosity in steps of 10 years.

Total vegetation cover for the static and dynamic scenarios was calculated as the fraction of cells containing vegetation of any type at the end of each year, before mortality. Dynamic vegetation was split into three stages: seedling (1 year old), bush (2–10 years old) and forest (older than 10 years). If multiple vegetation types with different ages occurred in one grid cell, the maximum age was taken to show the succession in age. Mortality by flooding, desiccation, uprooting, burial or scour was calculated per vegetation type and for each life stage.

Results

River morphology

The reference scenario without vegetation first shows lateral expansion and longitudinal migration of the meander bends, followed by an upstream chute cut-off after approximately 100 years (Movie S1, supporting information). This cut-off initiates a sequence of downstream cut-offs, which eventually lead to the formation of a mostly straight channel with low sinuosity (Figure 5A and 6C). The median detrended bed level first decreases rapidly and then settles around 0.2 m (Figure 6A). However, the 5th percentile of the bed level increases sharply after the first cut-off (Figure 6B), which indicates that the floodplain is generally eroding while the deep parts of the channels become shallower after each chute cut-off. Maximum water levels are fluctuating more in the first half of the run as a function of channel sinuosity and decrease after that as the system develops towards a low sinuous river in the second part of the run (Figure 6D).

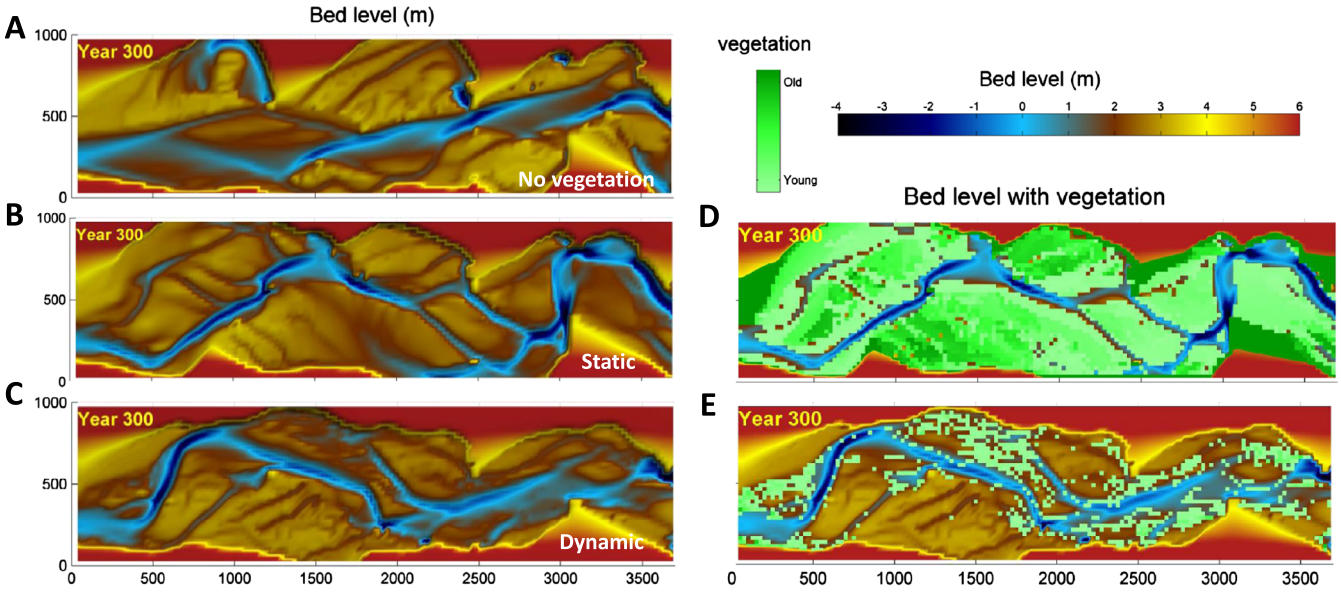

Figure 5. Bed level, vegetation cover and vegetation age after 300 years. (A) Scenario without vegetation. (B) Static vegetation scenario. (C) Dynamic vegetation scenario. (D) Vegetation age overlain on bed-level map for the static vegetation scenario. Here, vegetation colonizes each year anew and the age therefore indicates a stability in settlement location instead of actual age. (E) Vegetation age overlain on bed-level map for the dynamic vegetation scenario. This figure is available in colour online at wileyonlinelibrary.com/journal/espl

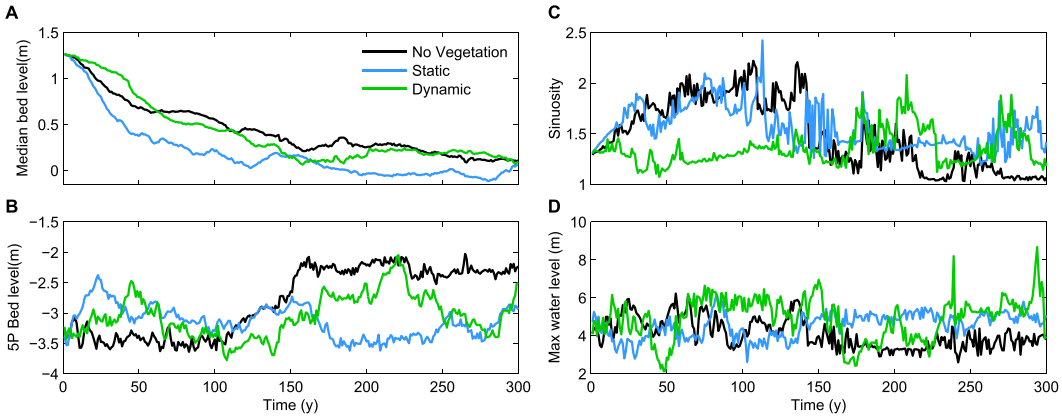

Figure 6. Time series of morphodynamics sampled at the end of each year for the scenarios without vegetation, with static vegetation and with dynamic vegetation. All values were calculated excluding 500 m from the upstream and downstream boundaries to compensate for boundary effects. (A) Median bed level. (B) 5th percentile bed level indicative of channel depth. (C) Sinuosity of the main channel. (D) Maximum water levels during flood cross-sectionally averaged in the centre of the reach. This figure is available in colour online at wileyonlinelibrary.com/journal/espl

The scenario with static vegetation shows a highly sinuous, meandering river with a lateral expansion (Figure 5B and Movie S2, supporting information). Initially, distinct morphological features like chute cut-offs and oxbow lakes are formed, which are similar to those visible on aerial photos of the River Allier (Figure 7A). Similar to the scenario without vegetation, the median bed level decreases throughout the run but at the highest rate of all scenarios (Figure 6A). The 5th percentile bed level fluctuates over time, indicating subsequent erosion and aggradation of the channels (Figure 6B). The sinuosity increases in the first half of the run and becomes more stable in the second half of the run (Figure 6C), which is caused by the decreasing dynamics over time. The same trend is found in the maximum water level (Figure 6D).

The scenario with dynamic vegetation is comparable to the first half of the scenario with static vegetation, showing a dynamically meandering system with regular chute cut-offs (Figure 5C and Movie S3, supporting information). After each cut-off, meanders laterally increase in size again until the next cut-off. On average, the meander amplitude stays equal throughout the whole run. Chute cut- offs occur regularly and oxbow lakes are formed; these features are visually comparable to the River Allier (Figure 7A). The median bed level decreases throughout the run and the 5th percentile of the bed level follows a sinuous shape, although with a higher amplitude than the static scenario (Figure 6A, B). The same accounts for the maximum water level; a fluctuation over time with the highest amplitude of all scenarios (Figure 6D). The sinuosity follows a reversed pattern compared to the static scenario; first it stays relatively stable, but the fluctuation becomes higher in the second part of the run (Figure 6C). Contrary to the static scenario, in the dynamic vegetation scenario the active meandering behaviour of the river is maintained.

Bed-level distribution

Effects of vegetation on morphological development are summarized in bed-level distributions (Figure 8). The initial distribution is bimodal, with a high bed-level peak for the initial floodplain and valley and a low bed-level peak for the sinuous channel carved into the floodplain. All scenarios show a similar development in that the floodplains are eroded over time. Differences arise because of vegetation development.

The dense, static vegetation leads to concentration of flow in the channels, shown as the highest and narrowest peak in the distribution relative to the unvegetated scenario (Figure 8, middle graphs). Furthermore, as the vegetation is reset every year, lateral channel mobility is high enough to erode the higher parts of the floodplain, and multiple, anabranching channels further heighten the peak. The narrow peak of the dynamic scenario relative to the unvegetated case also shows the flow-focusing effect, but here the vegetation reduces the lateral channel mobility by leaving room for chute cut-offs, so that the higher part of the floodplain is more slowly removed (Figure 8, bottom graphs). Here, the main morphodynamic activity takes place on the point bars, leading to a distribution with more equal modes than in the unvegetated and static vegetation cases.

The effect of vegetation becomes even more clear when a cross-section is made of a typical meander bend (Figure 9). The bed level of the scenario without vegetation develops

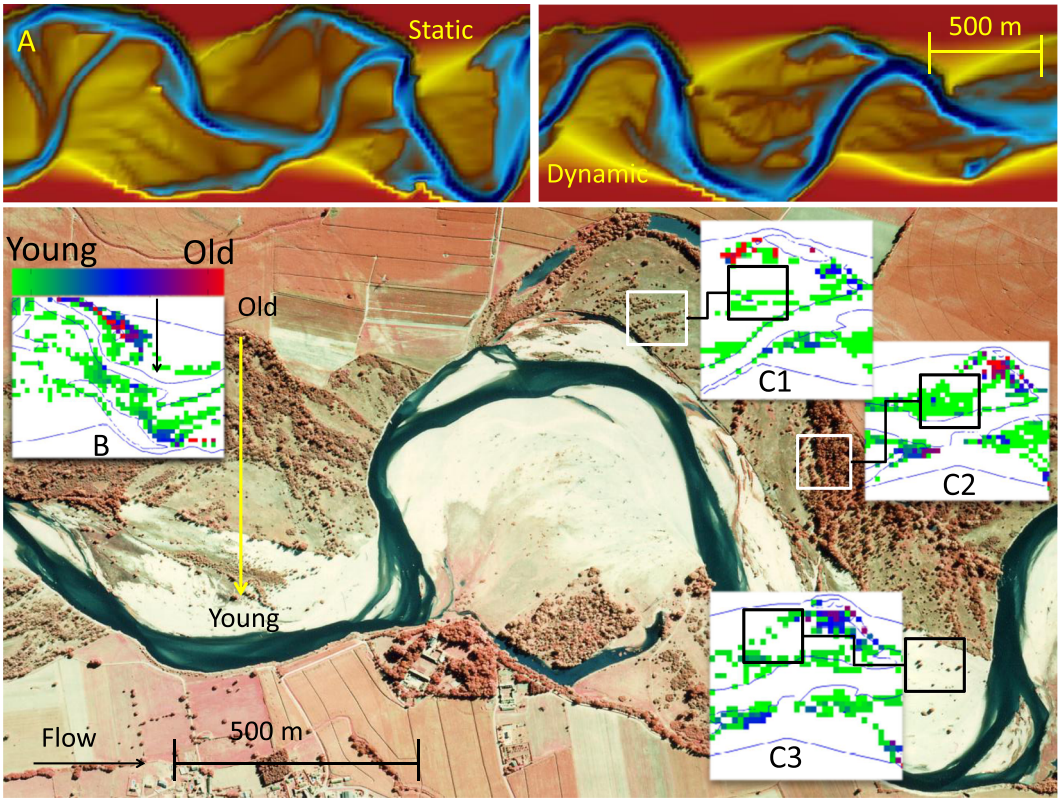

Figure 7. Comparison of morphological features, vegetation patterns and age distribution between aerial photos of the River Allier and model results. (A) River morphology of the static scenario (year 102) on the left and the dynamic scenario (year 109) on the right. Both scenarios show similar features compared to the River Allier, i.e. chute cut-offs and oxbow lakes. (B) Trends in vegetation age distribution of the dynamic scenario, with old vegetation on the higher parts of the point bars and younger vegetation closer to the channel. (C) Typical vegetation patterns of the dynamic scenario compared by considering basic shapes i.e. stripes (C1), areas (C2) and dots (C3). These model results are for Salicaceae species only, whereas the aerial photograph cannot distinguish between old Salicaceae vegetation and other species. This figure is available in colour online at wileyonlinelibrary.com/journal/espl

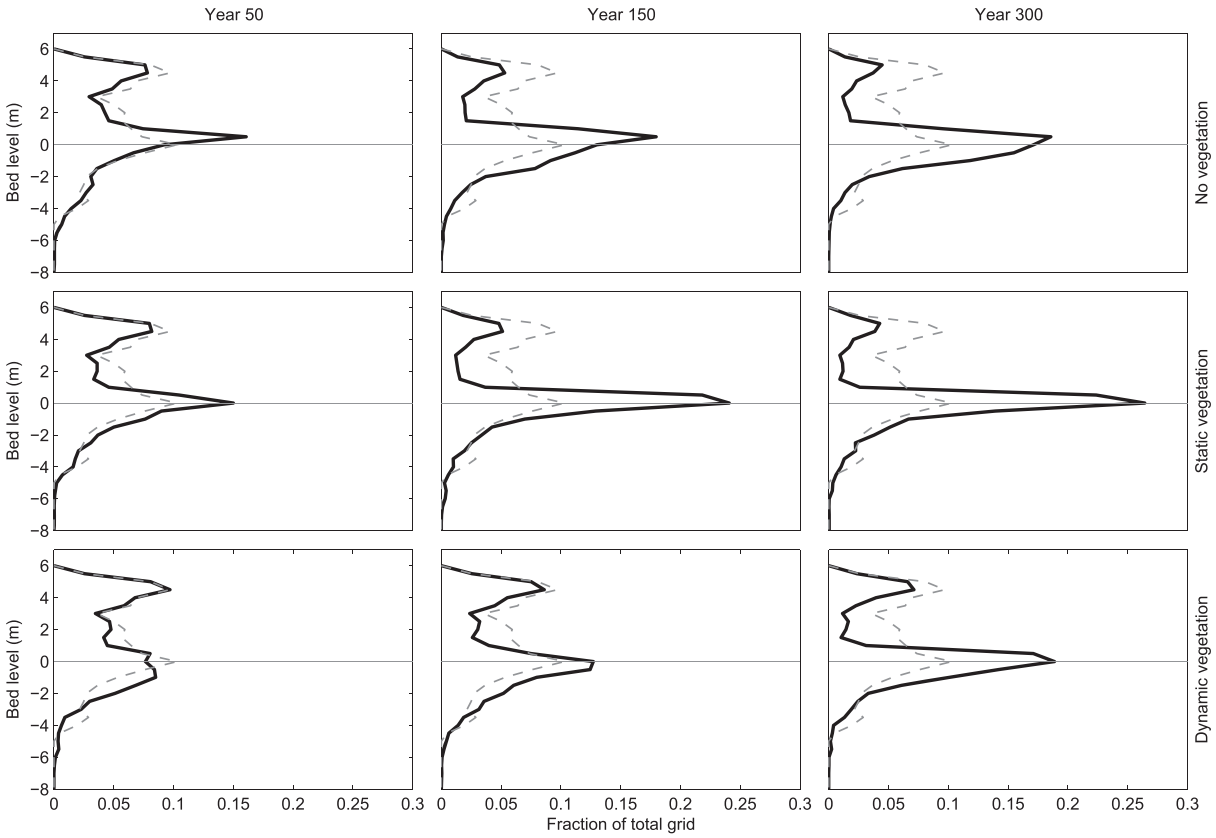

Figure 8. Distributions of detrended bed level over time for the three basic scenarios. The dashed line indicates the initial bed-level distribution after 1 year.

into a wide, shallow channel in a relatively smooth floodplain (Figure 9A), while the other scenarios with vegetation develop into deeper, tighter channels (Figure 9B, C). This figure also shows a direct contrast between the static and the dynamic scenario where the static scenario displays a floodplain with sharper transitions, while the transitions are more gradual in the dynamic scenario. Clearly, vegetation has two distinct effects on morphology that depend sensitively on the vegetation parameters. In the first place, presence of vegetation leads to focusing of the flow, resulting in deeper channels. However, lateral channel dynamics are mostly affected by vegetation removal, where static vegetation causes high lateral migration activity and a more stepwise topography compared to a lower lateral migration and gradual floodplain in the case with dynamic vegetation.

The clear differences in river morphology between all scenarios become tangible when scenario statistics are compared from 100 years onwards (Table III). As shown by previous results, the unvegetated scenario develops into a straight channel with a low sinuosity. The river becomes shallower and wider, increasing the surface on which sediment transport can take place, eventually developing into a system with a higher sediment transport rate and a higher median bed level than in the scenarios with vegetation. Vegetation leads to focusing of flow in the channel causing deeper channels which are most intense in the static scenario. This scenario contains the highest vegetation density, maximizing the hydraulic roughness and decreasing flow velocities on the floodplain and minimizing the area over which sediment transport can take place, resulting in the lowest sediment transport rate. Because vegetation cover is high, sinuosity is still higher than in the dynamic scenario, but the river dynamics are actually decreasing. This is especially clear in the last part of the run, which is supported by a lower meander migration rate than the dynamic scenario (Table III and Movie S2, supporting information). In the default dynamic scenario, vegetation development is less dense and very dynamic, leaving room for occasional chute cut-offs, leading to a dynamic meandering system with the highest meander migration rate and still a high sinuosity (Table III and Movie S3, supporting information). This result further supports that dynamic vegetation development is a prerequisite for modelling a dynamic meandering system.

Vegetation

The static and dynamic vegetation scenarios show large differences in vegetation settlement patterns. In the scenario with static vegetation, the floodplains are immediately densely vegetated from the start of the simulation and remain so throughout the run (Figures 5D and 9B). In the scenario with dynamic vegetation, the floodplains are less densely vegetated and consist of vegetation with different ages and densities (Figures 5E and 9C). In some years the number of seedlings increases rapidly. This shows that colonization success varies from year to year. However, most seedlings die again the next year. This is clearly shown in the peaks of the vegetation cover (Figure 10A). In the static scenario, there are also peaks in the vegetation cover (Figure 10B). These peaks in the static scenario are caused by changes in river morphology and changes in discharge during the time of colonization which create annual changes in dry areas for vegetation settlement. The total median vegetation cover of the dynamic scenario is around 10%, while the total median cover of static vegetation is about 81% (Figure 10C). Compared to empirical data from Geerling *et al.* (2006), showing about 16% cover, the static vegetation scenario is a factor of 5 higher, while the dynamic scenario shows a slightly lower vegetation cover with a factor

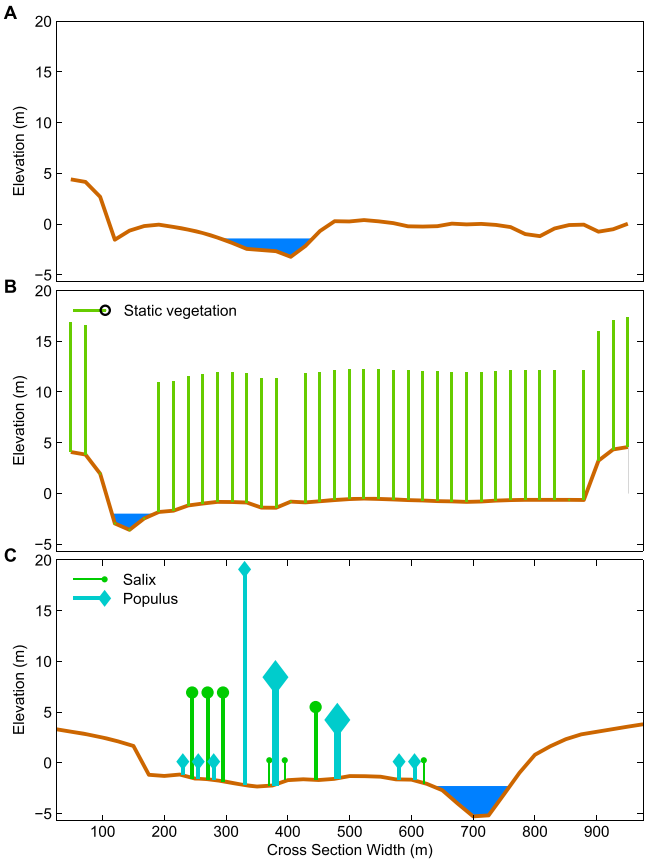

Figure 9. Cross-sections of a typical meander bend with bed level and vegetation for all scenarios. (A) Scenario without vegetation, year 285. (B) Scenario with static vegetation, year 125. The size of vegetation stems is the actual size of the vegetation used in the model. (C) Scenario with dynamic vegetation, year 205. The size of vegetation stems is the actual size of the vegetation used in the model. The thickness of the stems gives an indication of the frontal area (number of stems × width of the stem). Thicker stems represent a larger frontal area. This figure is available in colour online at wileyonlinelibrary.com/journal/espl

of 1.6. However, it should be taken into account that Geerling *et al.* (2006) did not map Salicaceae species exclusively, consequently leading to a higher vegetation cover.

The settlement locations of the *Salix* and *Populus* seedlings show that in years with average settlement conditions *Salix* seedlings that settle and survive at lower elevation (respectively −1.5 and −2 m) than *Populus* seedlings (respectively −1 and −0.5 m) (Figure 11). This corresponds to the higher tolerance of *Salix* for wetter conditions and higher tolerance of *Populus* for dryer conditions. Eventually this results in an average settlement of −1 m for *Salix* and −0.5 m for *Populus*. These results also show that the range of seedlings survival is smaller than the initial range of settled seedlings, but in years with high vegetation settlement this range expands proportionally with suitability for settlement.

The main mortality cause for *Salix* and *Populus* seedlings is desiccation, followed by flooding and uprooting due to high flow velocities. Scour and burial cause less mortality in both vegetation types, with an even negligible scour mortality for *Populus*. When seedlings survive the first year, mortality drops drastically to approximately 15% in the bush stage (2–10 years old) and 5% in the forest stage (>10 years old). The main causes of mortality in these stages are desiccation and flooding, while scour is an occasional cause of mortality.

The static and dynamic vegetation scenarios produced quite different vegetation patterns, which we here compare with patterns on aerial photos of the River Allier (Figure 7). In the static scenario there is a dense vegetation cover, while the dynamic scenario creates vegetation patterns with different shapes and sizes. To be able to compare vegetation patterns from the model with aerial photos, we considered three simple shapes, namely spots, stripes and areas. Here we define a spot as one vegetated grid cell, stripes as areas with vegetation which are more than twice as long as they are wide and areas as all other shapes. The position and orientation of these shapes on a point bar determine the vegetation pattern. The vegetation patterns in the static scenario contain one dense area shape (Figure 5D). In contrast, the vegetation pattern in the dynamic scenario well resembles the pattern from the aerial photos of the River Allier because all characteristic shapes can be found and are comparable in size (Figure 7C).

There is also a clear age distribution of vegetation in the dynamic scenario. The oldest vegetation is generally found around oxbow lakes and the youngest vegetation on the lower parts of the point bars, which is consistent with vegetation patterns along the River Allier (Figures 5E, 7B and 9C). Although Salicaceae species cannot be recognized within the dense vegetation patches on the aerial photograph, experience from the field shows that older Salicaceae trees are found in large quantities along oxbow lakes. In the static scenario there is no actual age distribution because the vegetation colonizes each year and therefore represents an annual plant rather of a perennial (Figure 9B). Here the age distribution can be expressed as a factor for recolonization in the same cell each year. However, this is more a reflection of the timing of morphological activity than plant age since plant growth is not taken into account in this scenario.

Vegetation interaction with morphodynamics

To test the sensitivity of the patterns in morphology and vegetation resulting from the model and to further support the findings of our main scenarios, a range of scenarios were analysed representing 10 vegetation types with different ecological strategies. This method was chosen as opposed to a random sampling type of approach, because it gives specific information on the suitability of the model for representing

Table III. Morphological and vegetation statistics of the main scenarios calculated from 100 to 300 years to minimize the effect of initial conditions

Parameter	Unit	No vegetation	Static vegetation	Dynamic vegetation
Median sinuosity	—	1.18	1.41	1.38
Median bed level	m	0.26	−0.01	0.19
Median sediment transport rate	$m^3/s/m$	1.52×10^{-6}	3.83×10^{-7}	7.24×10^{-7}
Meander migration rate	m/y	30	73	98
Median vegetation cover	%	0.0	81.6	10.0
Temporal variation in vegetation cover (P95–P5)	%	0.0	5.5	15.8

different types of vegetation in different settings rather than a large range of values for general parameters. The parameter values for the scenarios are presented in Table IV. The scenarios include vegetation types with a fast initial growth and short life span (S1), slow initial growth and long life span (S2), sensitive seedlings (S3), resistant seedlings (S4), high drag (S5), low drag (S6), early dispersal timing (S7), late dispersal timing (S8), dense vegetation (S9) and sparse vegetation (S10).

The results show a broad range in river morphologies and vegetation cover (Figures 12 and 13). The median vegetation cover differs between scenarios and all scenarios fluctuate around field data with an outlier upwards (scenario S4, resistant seedlings) and downwards (scenario S7, early dispersal, where vegetation does not exceed the age of 1). We find that increasing vegetation cover decreases median sediment transport and median bed level, which supports the findings of the main scenarios (Table V). The decreasing effect of dense vegetation cover on morphodynamics in the static scenario is further supported in scenario S4 with resistant seedlings (Figure 13 and Table V). In this scenario, the meander migration rate is the lowest of all dynamic scenarios.

Changes in temporal vegetation dynamics of all dynamic scenarios expressed as the difference between the 95th and the 5th percentile of the vegetation cover for all years, rather than the median vegetation cover, seem to have a more pronounced decreasing effect on the sediment transport rate. When the effects of the different life stages of vegetation are separated, it becomes clear that the bush stage has the largest decreasing effect on the sediment transport rate.

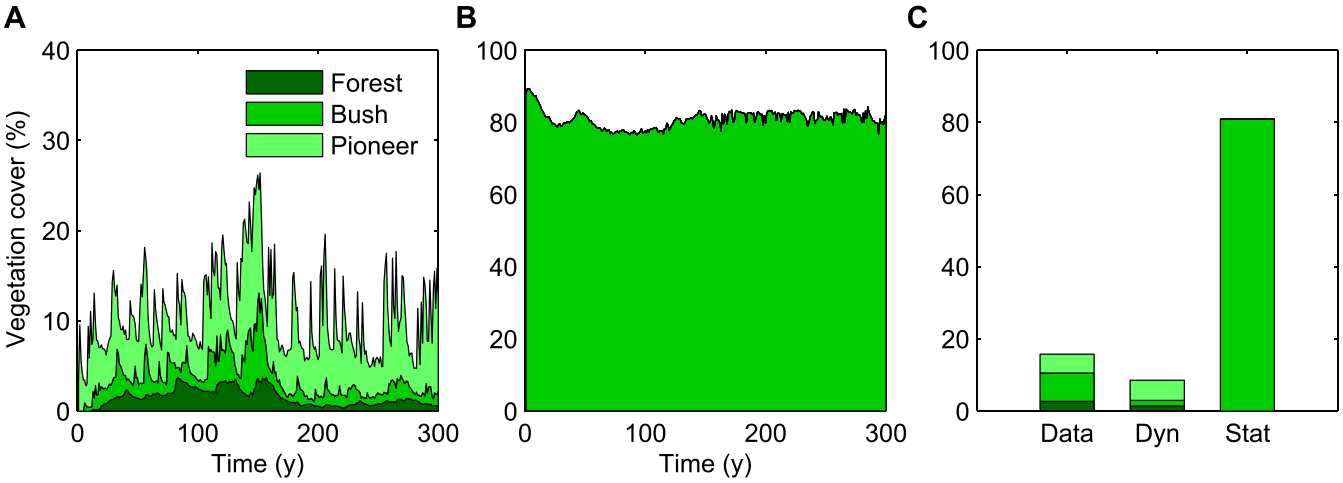

Figure 10. (A) Total median vegetation cover of the dynamic vegetation scenario per year per vegetation class (pioneer = 1-year-old seedlings, bush = 2–10 years, forest = >10 years). (B) Total cover in the static vegetation scenario per year. (C) Median vegetation cover calculated from year 25 until year 300 to let forest develop first. 'Data' is field data from (Geerling *et al.*, 2006), 'Dyn' is dynamic scenario and Stat' is static scenario). Note that A has a smaller vertical scale compared to B and C. This figure is available in colour online at wileyonlinelibrary.com/journal/espl

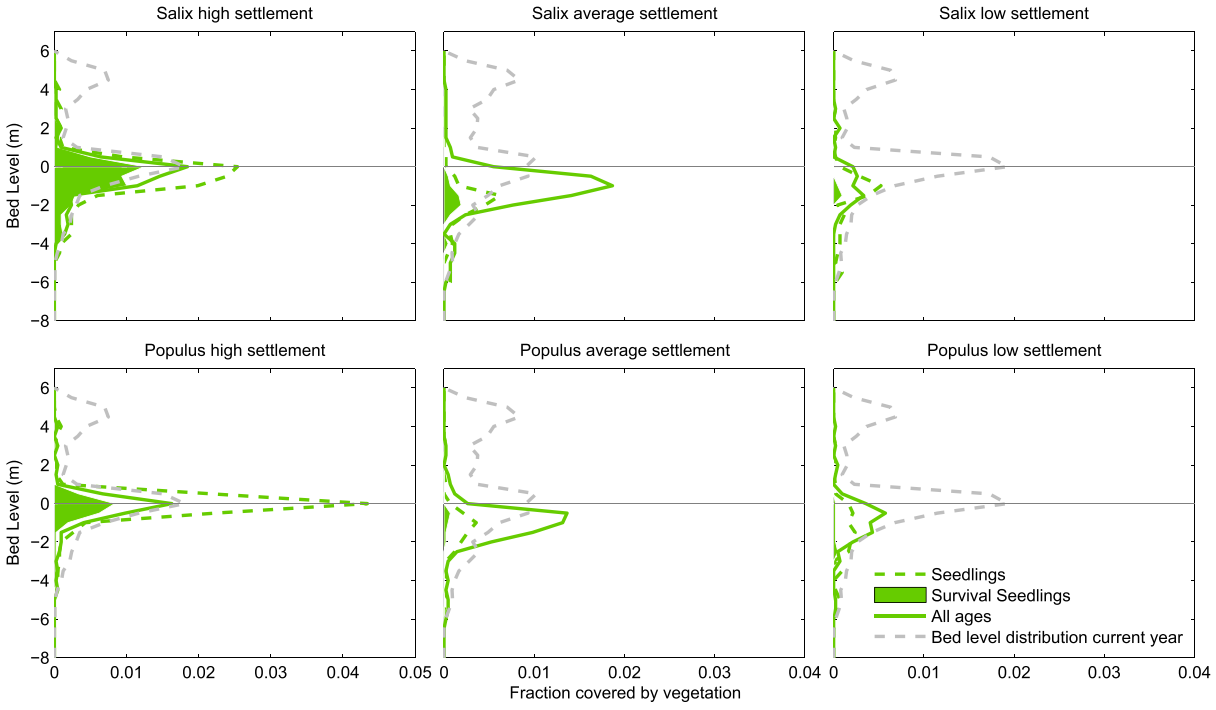

Figure 11. Vegetation cover of *Salix* (top) and *Populus* (bottom) as a function of detrended bed level for years of low (left), average (middle) and high (right) settlement rates in years 206, 90 and 282, respectively. Dashed green lines show seedling settlement in a year, filled areas show seedlings that survived in that year and solid lines show survival of all age classes until that year. The grey dashed lines represent the bed-level distributions of the corresponding years. This figure is available in colour online at wileyonlinelibrary.com/journal/espl

Table IV. Vegetation parameter values for the sensitivity scenarios. Only parameter values are shown that deviate from our preferred default dynamic vegetation scenario in Table II. The scenarios are: fast (S1) and slow (S2) initial growth with short (S1) and long (S2) life span, sensitive seedlings (S3) and resistant seedlings (S4), high (S5) and low (S6) drag coefficient, earlier (S7) and delayed (S8) dispersal timing, densely (i.e. high stem density) (S9) and sparsely (i.e. low stem density (S10) vegetated patches. 'Seed' is the abbreviation for the seedling stage and 'Other' are the other life stages

	Des. thresh.[a] seed (days)		Des. thresh. other (days)		Fl. thresh.[b] seed (days)		Fl. thresh. other (days)		Flow thresh.[c] seed (m/s)		Flow thresh. other (m/s)	
	Salix	*Populus*	*Salix*	*Populus*	*Salix*	*Populus*	*Salix*	*Populus*	*Salix*	*Populus*	*Salix*	*Populus*
S3	12.5	17.5	95	105	35	30	130	120	0.275	0.275	3.5	3.5
S4	50	70	365	365	140	120	365	365	1.1	1.1	14	14
Default	25	35	190–365	210–365	70	60	260–365	240–365	0.55	0.55	7.0–15.0	7.0–15.0
	Max. age (yrs)		Ini. root length (m)		Ini. shoot length (m)		Growth factor root		Growth factor shoot			
	Salix	*Populus*	*Salix*	*Populus*	*Salix*	*Populus*	*Salix*	*Populus*	*Salix*	*Populus*		
S1	10	25	0.2	1.0	0.5	0.2	1.5	1.8	20.4	21.8		
S2	120	300	0.05	0.2	0.125	0.05	0.73	1.0	9.8	12.1		
Default	60	150	0.1	0.5	0.25	0.1	0.85	1.15	11.5	14		
	c_d seed	c_d other	Timing seed dispersal (month)		Num. stems/m^2 seed		Num. stems/m^2 other					
			Salix	*Populus*	*Salix*	*Populus*	*Salix*	*Populus*				
S5	0.5	0.75	Default	Default	Default	Default	Default	Default				
S6	2	3	Default	Default	Default	Default	Default	Default				
S7	Default	Default	March	Februari	Default	Default	Default	Default				
S8	Default	Default	September	August	Default	Default	Default	Default				
S9	Default	Default	Default	Default	50	50	30	26				
S10	Default	Default	Default	Default	12	12	7	6				

[a]Desiccation threshold.
[b]Flooding threshold.
[c]Flow velocity threshold.

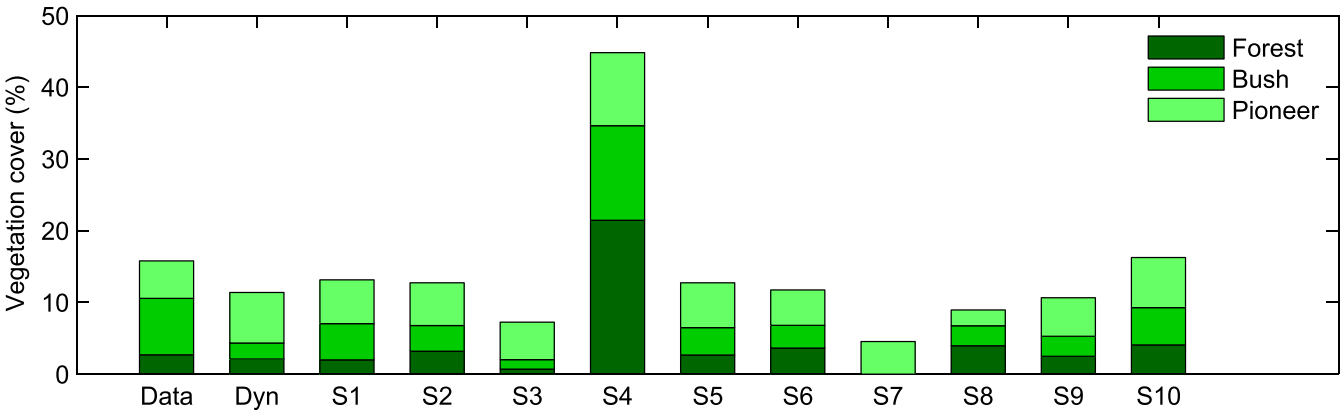

Figure 12. Vegetation age distribution of all dynamic scenarios compared to field data. Median vegetation cover of three age classes (pioneer = 1 year, bush = 2–10 years and forest = older than 10 years). 'Data' is field data from Geerling *et al.* (2006), 'Dyn' is the main dynamic scenario and S1–S10 are all the dynamic scenarios in the sensitivity analysis. Vegetation cover is calculated from year 25 until year 150.This figure is available in colour online at wileyonlinelibrary.com/journal/espl

Discussion

Morphodynamics

We find that dynamic vegetation with a range of time-variable traits, as opposed to static vegetation, causes high channel sinuosity with repeated chute cut-offs and bar–floodplain conversion that are similar to those in our study area. In general, vegetation in our static and dynamic scenario causes a single-thread river, despite the repeated chute cut-offs, as opposed to the scenario without vegetation (Figure 5), which transforms to a rather straight channel. This finding is in general agreement with several other modelling studies (Nicholas, 2013; Crosato and Saleh, 2011) and flume experiments (Tal and Paola, 2010; Van Dijk *et al.*, 2013) where uniformly distributed vegetation promotes the formation of a single-thread channel. Our results show a dense vegetation cover causing the flow to concentrate in the channel, resulting in deeper, narrower channels (Figure 8). The same effect has been reported by flume experiments with uniform vegetation settlement (Van Dijk *et al.*, 2013), field data and modelling studies (Temmerman *et al.*, 2007; Murray *et al.*, 2008).

The vegetation settlement conditions in the static scenario results in the most densely vegetated floodplains (Figures 9B and 5D; Movie S2, supporting information), creating a stronger flow concentration into channels, leading to sharper meander bends, a higher sinuosity and a floodplain with steeper bed-level transitions than the scenario with dynamic vegetation. In the dynamic scenario, chute cut-offs are created more frequently and gradually, because the vegetation development on the point bars occurs gradually and is less dense and more diverse (Figures 9C and 5E; Movie S3, supporting information), while in the static scenario chute cut-offs are more stepwise because they are forced by the vegetation settlement conditions. Initially, both scenarios show quite actively meandering patterns, but in the second half of the static run the dynamics decrease drastically (Movie S2, supporting information). This indicates that the static vegetation system is developing towards a static state, perhaps comparable to a river in a tropical climate where the dense vegetation dominates over morphodynamic processes in determining river morphology. So, in the scenario with static vegetation, river morphology is imposed by vegetation, while in the dynamic scenario there is a continuous dynamic interaction between morphodynamics and vegetation, leading to active meandering behaviour throughout the whole run. This behaviour was observed not only in our default dynamic scenario but also in the other dynamic scenarios (Figure 13).

Until now it has been difficult to model natural, dynamically meandering rivers. Simplistically speaking, meandering is caused by a combination of outer bank erosion and inner bend deposition and stabilization in which bar–floodplain conversion, i.e. by vegetation or cohesive material, is required to sustain high-sinuosity meandering. This bar–floodplain conversion mechanism observed in the field has rarely been included in advanced, numerical morphodynamic models. In the Delft3D model, for instance, there is no actual bar–floodplain conversion mechanism, while in other advanced numerical meander models (e.g. Nays2D) the bar–floodplain conversion is implemented as a simplistic threshold value related to water level (Schuurman *et al.*, 2013). We show that natural bar–floodplain conversion emerges as a result of our dynamic vegetation model, and this is sufficient to form a dynamic meandering system.

Vegetation

We show that natural vegetation patterns emerge from the modelled interaction between dynamic vegetation and morphodynamics. The modelled patterns are similar to those observed on aerial photos of our study area (Figure 7C). We distinguished three basic vegetation shapes on the aerial photo, i.e. dots, stripes and areas, which are all found on point bars in the dynamic scenario. Moreover, the age distribution across the floodplain is similar to the aerial photos; older vegetation is found on the higher parts of the point bars near oxbow lakes and younger vegetation is found on the lower areas. In hindcast, this is a realistic result considering that new vegetation settlement takes place on the lower parts of the point bars and, when the channel continues to migrate, vegetation can grow older but still needs a certain amount of water to survive. Also the vegetation age categories agree with empirical data derived from aerial photos of the River Allier (Geerling *et al.*, 2006; Figure 10C). The modelled vegetation age distribution shows slightly younger ages than the empirical vegetation age distribution derived for the River Allier, but since we only include Salicaceae species while Geerling *et al.* (2006) included all vegetation types, we probably overestimate the abundance of Salicaceae vegetation. The static vegetation scenario does neither model diversity nor an age distribution, but is merely a dense cover with uniform age and one set of properties. Clearly, dynamic vegetation results in

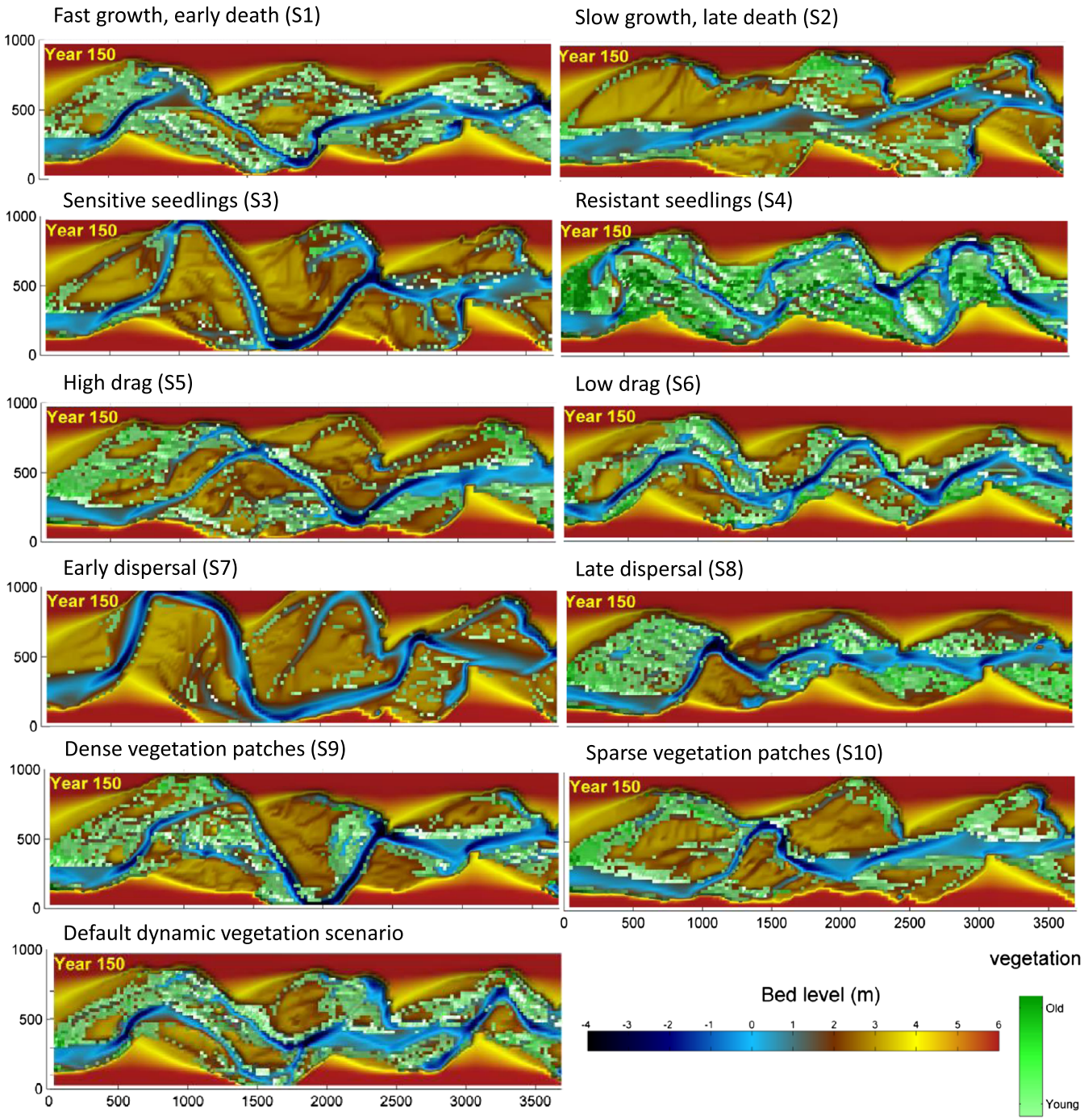

Figure 13. Bed level and vegetation cover after 150 years of the following scenarios for sensitivity analysis. The scenarios are: fast (S1) and slow (S2) initial growth with short (S1) and long (S2) life span, sensitive seedlings (S3) and resistant seedlings (S4), high (S5) and low (S6) drag coefficient, earlier (S7) and delayed (S8) dispersal timing, densely (i.e. high stem density and cells completely filled with vegetation) (S9) and sparsely (i.e. low stem density and cells half filled with vegetation) vegetated patches (S10). This figure is available in colour online at wileyonlinelibrary.com/journal/espl

realistic vegetation patterns and age distribution whereas static vegetation does not.

Varying dynamic vegetation properties generates a range of river morphologies with different bed-level distributions, sediment transport rates, sinuosity and meander migration rates (Figure 13 and Table V). Vegetation settlement location, density and survival are influenced by basic vegetation parameters. By introducing multiple species we made it possible to study the effect of different vegetation types with different morphologies, settling location and behaviour on the spatial vegetation pattern and river morphology. Furthermore, by including several life stages within a vegetation type, the growth of vegetation is represented in a more realistic way. Rather than using one vegetation type with static properties, modelled vegetation develops and grows according to its natural behaviour. In particular, seedlings are very susceptible to morphodynamic pressures, but once they survive the colonization phase they increase in strength and ability to withstand more pressure, creating a hysteresis effect which is also observed in the field (Gurnell, 2014). These changes in vegetation settlement and vegetation properties create a heterogeneous floodplain vegetation, which in turn causes local differences in flow and subsequently erosion and sedimentation patterns, leading to a different river morphology. An effect

of different vegetation settlement strategies on river morphology is also indicated in the modelling study by Nicholas (2013) where different vegetation colonization rates produce different channel pattern dynamics. Moreover, Bertoldi *et al.* (2011) show that differences in vegetation settlement and growth rate alter the shape of the observed bed-level distribution of reaches in the Tagliamento River.

Vegetation survival determines the vegetation pattern in the long term. Differences in vegetation survival create distinct vegetation patterns leading to different river morphology. This is clearly shown when the patterns in vegetation and river morphology are compared between scenarios with different survival characteristics (scenarios S3 and S4 in Figure 13). The sensitive seedling scenario (S3) shows a low vegetation cover while the resistant seedling scenario (S4) generates a high vegetation cover, both resulting in different river morphology and dynamics (Table V). In the default dynamic scenario there is a zonation in *Populus* and *Salix* settlement, which is created by a different sensitivity of the two species to flooding and desiccation combined with different morphological and developmental properties (Figure 11). The range of morphological pressures that can cause vegetation mortality, i.e. flooding, desiccation, uprooting, scour and burial, also led to several interesting trends. For instance, *Populus* is less susceptible to scour because of its larger taproot combined with an earlier dispersal period, causing the seeds to be deposited at higher elevations, which are less affected by morphodynamic activity. The importance of morphological traits and the dynamics of these traits in vegetation survival are also shown by Kui *et al.* (2014) in a large experiment in a meandering flume containing two types of vegetation with different morphological traits. These vegetation types show differences in sensitivities for and interaction with morphodynamic parameters. This is similar to our case with *Salix* and *Populus* types containing distinct morphological traits influencing their settlement and survival (Figure 11 and Table II). Our multi-species approach with different dynamic vegetation characteristics addresses a number of important issues raised by several authors (Kui *et al.*, 2014; Bertoldi *et al.*, 2014; Camporeale *et al.*, 2013) concerning the realistic description of riparian ecosystems, and is therefore a step forward in modelling the interaction between vegetation and morphodynamics compared to other advanced physics-based morphodynamic modelling studies that only included vegetation removal when cells were eroded (Nicholas, 2013) or Shields forces exceeded a critical value (Bertoldi *et al.*, 2014).

In this study we have chosen to include only those riparian species that are the primary eco-engineers that colonize the bare substrate close to the river channel. Other vegetation types growing on the higher parts of the floodplain (e.g. hardwood forest, bush, herbs and grass) would occasionally affect the morphodynamics during the highest floods. Ignoring these in the model means that for the highest floods these areas are slightly more susceptible to sedimentation and bend cut-offs than would be the case in nature.

Vegetation and rooting affect bank stability, and hence the type of vegetation on the outer banks affects the meander migration rate. This means that our model may overestimate bend migration and overall morphodynamics due to the absence of hardwood forest on the older, higher parts of the floodplain. However, as sinuosity increases, the capacity of the flow reduces and water level increases until chute cut-off takes place, after which the river moves away from the forest. We therefore expect this effect to be minor. Future modelling may resolve the effects of different types of eco-engineers on channel migration.

Table V. Statistics of vegetation and morphodynamic parameters values for all dynamic scenarios calculated from 25 to 150 years

Parameter	unit	Dyn[a]	S1	S2	S3	S4	S5	S6	S7	S8	S9	S10
Median vegetation cover	%	11.6	20.1	18.5	11.0	61.6	18.4	17.6	6.2	12.5	17.1	24.4
Dynamics in vegetation cover	95P–5P	14.2	30.6	22.5	16.2	32.0	17.1	24.2	3.3	18.6	22.4	21.6
Median *Salix* cover	%	10.7	12.2	13.4	3.3	40.6	12.8	12.5	6.2	11.0	10.3	19.2
Median *Populus* cover	%	7.2	8.6	9.2	8.1	34.2	8.8	9.0	0.0	2.1	8.2	13.1
Median pioneer cover	%	7.1	6.1	6.0	5.2	10.2	6.3	4.9	4.5	2.2	5.4	7.0
Median bush cover	%	2.2	5.1	3.6	1.3	13.2	3.8	3.2	0.0	2.8	2.8	5.2
Median forest cover	%	2.1	2.0	3.2	0.7	21.5	2.7	3.6	0.0	3.9	2.5	4.1
Median sinuosity		1.29	1.18	1.44	1.44	1.43	1.33	1.24	1.73	1.13	1.35	1.35
Median bed level	m	0.50	0.43	0.63	0.67	0.18	0.47	0.60	0.45	0.60	0.29	0.43
Median sediment transport rate	$m^3/s/m$	7.1E−07	3.2E−07	6.1E−07	7.6E−07	7.4E−08	5.4E−07	5.7E−07	1.2E−06	5.4E−07	5.3E−07	5.5E−07
Median meander migration rate	m/y	87.8	101.4	105.2	100.0	56.6	152.6	81.4	115.0	122.8	158.2	133.4

[a] Dyn is the main dynamic scenario.

A comparison of vegetation statistics of all scenarios with morphodynamic statistics demonstrates a quantitative interaction between dynamic vegetation and median sediment transport rate as representing morphodynamics (Table V): when vegetation cover increases, sediment transport is reduced. This is caused by increased hydraulic resistance, leading to decreased flow velocity on the point bars and more focusing of flow towards the main channel, thereby reducing the area over which sediment transport can take place. Interestingly, we find that not the median vegetation cover in itself, but rather the natural changes of vegetation cover over time, expressed as the difference between the 95th and the 5th percentiles, has the largest effect on the sediment transport rate (Table V). When the vegetation types are split into groups with different morphological properties, it becomes clear that the bush stage of the vegetation is the main driver of this process. This is not surprising, since this vegetation stage contains the largest frontal area and therefore causes the highest hydraulic resistance (Table II). These results confirm a quantitative interaction between vegetation and morphodynamics and show that dynamic vegetation properties influencing settlement, density and survival are the main drivers in creating different river morphologies.

Our results imply that changes in species distribution with different life history strategies and morphological traits have profound effects on river morphology. This can be the case, for instance, in areas suffering from invasive species where one species becomes dominant and replaces the native species (Tickner *et al.*, 2001). Also management strategies such as grazing affect river morphology when it removes certain palatable vegetation types which are not able to survive until the bush stage because they are eaten before reaching maturity. This in turn would favour the less palatable species which have different traits and consequently a different interaction with morphodynamics. Exciting future research directions would be to investigate how changing boundary conditions affect the interaction of vegetation and river morphology and, through this, the dynamics of other species inhabiting the floodplain, and how human pressures and river rehabilitation measures influence these processes in the long term.

Conclusions

Our modelling study shows that dynamic vegetation, as opposed to static vegetation, produces vegetation patterns and vegetation age distribution that are similar to patterns observed from aerial photos of our study area. All characteristic vegetation shapes occur on the floodplain of the dynamic scenario, while in the static scenario vegetation develops into one dense area. Furthermore, the dynamic scenario shows a lateral age distribution across the floodplain, with older vegetation at higher elevations near oxbow lakes and young vegetation closer to the channel.

Dynamic vegetation creates and maintains an active meandering system, whereas the static vegetation reduces the morphodynamics over time and transforms the river into a static, vegetation-dominated state. Without vegetation, the river develops into a straight, broad and shallow channel with low sinuosity. Vegetation concentrates the flow in the channel, creating deeper, narrower channels, the effect of which is most pronounced in the static scenario because of the higher vegetation cover. A dynamic, heterogeneous vegetation cover reduces the lateral migration by increasing the number of chute cut-offs, increasing the meander migration rate and creating a smoother floodplain compared to the static vegetation.

We show a quantitative interaction between vegetation and morphodynamics, in that increasing vegetation cover and temporal variation in vegetation cover decreases median sediment transport rates and median bed levels. Differences in vegetation settlement conditions, density and survival create distinct patterns in river morphology, showing that vegetation properties and dynamics are important drivers in shaping different river morphologies.

The method presented in this study offers the combination of a well-verified morphodynamic model and a verifiable vegetation model, which is essential in long-term prediction of river–floodplain evolution in scientific and practical applications.

Acknowledgements— We thank C. Camporeale, the Associate Editor and an anonymous reviewer for reviewing and fine-tuning the manuscript. Filip Schuurman is gratefully acknowledged for his help in coupling Delft3D and the new vegetation model in Matlab. Jonne Kleijer produced the script to create the initial bed levels. Erik Mosselman (Deltares) and Tom Buijse (Deltares) are thanked for useful discussion. This work was funded by REFORM (FP7 Grant Agreement 282656). The authors contributed in the following proportions to conception and design, model running, analysis and conclusions, and manuscript preparation: MvO (40, 100, 75, 75%), MGK (30, 0, 15, 15%), GG (20, 0, 5, 5%) and HM (10, 0, 5, 5%). The online supporting information contains movies with model runs of the three basic scenarios.

References

Aberle J, Järvelä J. 2013. Flow resistance of emergent rigid and flexible floodplain vegetation. *Journal of Hydraulic Research* **51**(1): 33–45.

Baptist M, Babovic V, Rodriguez Uthurburu J, Uittenbogaard R, Mynett A, Verwey A. 2007. On inducing equations for vegetation resistance. *Journal of Hydraulic Research* **45**(4): 435–450.

Bertoldi W, Gurnell A, Surian N, Tockner K, Zanoni L, Ziliani L, Zolezzi G. 2009. Understanding reference processes: linkages between river flows, sediment dynamics and vegetated landforms along the Tagliamento river, Italy. *River Research and Applications* **25**: 501–516.

Bertoldi W, Gurnell AM, Drake NA. 2011. The topographic signature of vegetation development along a braided river: results of a combined analysis of airborne lidar, color air photographs, and ground measurements. *Water Resources Research* **47**(6): 1–13.

Bertoldi W, Siviglia A, Tettamanti S, Toffolon M, Vetsch D, Francalanci S. 2014. Modeling vegetation controls on fluvial morphological trajectories. *Geophysical Research Letters* **41**: 7167–7175.

Braatne J, Rood S, Heilman P. 1996. Life history, ecology and conservation of riparian cottonwoods in north America. In *Life history, Ecology, and Conservation of Riparian Cottonwoods in North America*, Stettler R, Bradshaw G, Heilman P, Hinckley T (eds), NRC Research Press: Ottawa; 57–85.

Braudrick C, Dietrich WE, Leverich GT, Sklar LS. 2009. Experimental evidence for the conditions necessary to sustain meandering in coarse-bedded rivers. *Proceedings of the National Academy of Sciences of the USA* **106**(40): 16936–16941.

Camporeale C, Ridolfi L. 2010. Interplay among river meandering, discharge stochasticity and riparian vegetation. *Journal of Hydrology* **382**(1–4): 138–144.

Camporeale C, Perucca E, Ridolfi L, Gurnell AM. 2013. Modeling the interaction between river morphodynamics and riparian vegetation. *Reviews of Geophysics* **51**(3): 379–414.

Canadell J, Jackson RB, Ehleringer JB, Mooney HA, Sala OE, Schulze ED. 1996. Maximum rooting depth of vegetation types at the global scale. *Oecologia* **108**(4): 583–595.

Corenblit D, Steiger J, Gurnell AM, Naiman RJ. 2009. Plants intertwine fluvial landform dynamics with ecological succession and natural selection: a niche construction perspective for riparian systems. *Global Ecology and Biogeography* **18**(4): 507–520.

Corenblit D, Baas A C, Bornette G, Darrozes J, Delmotte S, Ra Francis, Gurnell A M, Julien F, Naiman R J, Steiger J. 2011. Feedbacks

between geomorphology and biota controlling Earth surface processes and landforms: a review of foundation concepts and current understandings. *Earth-Science Reviews* **106**(3–4): 307–331.

Coulthard TJ, Hicks DM, Van De Wiel MJ. 2007. Cellular modelling of river catchments and reaches: advantages, limitations and prospects. *Geomorphology* **90**(3–4): 192–207.

Crosato A, Saleh MS. 2011. Numerical study on the effects of floodplain vegetation on river planform style. *Earth Surface Processes and Landforms* **36**(6): 711–720.

Curran JC, Hession WC. 2013. Vegetative impacts on hydraulics and sediment processes across the fluvial system. *Journal of Hydrology* **505**: 364–376.

Fotherby L, Huang J, Greimann B. Vegetation modeling with SRH-1DV. Predicting the interactions between flow, sediment and riparian research and development, Technical Report , US Department of the Interior Bureau of Reclamation, Denver, CO, 2012.

García-Arias A, Francés F. 2015. The RVDM: modelling impacts, evolution and competition processes to determine riparian vegetation dynamics. *Ecohydrology* (early view).

Geerling G, Ragas A, Leuven R, van Den Berg J, Breedveld M, Liefhebber D, Smits A. 2006. Succession and rejuvenation in floodplains along the river Allier (France). *Hydrobiologia* **565**(1): 71–86.

Gerritsen H, de Goede E, Platzek F, Genseberger M, van Kester J, Uittenbogaard R. 2007 Validation Document Delft3D-FLOW: a software system for 3D flow simulations, Technical Report , Deltares Delft.

Greet J, Angus Webb J, Cousens RD. 2011. The importance of seasonal flow timing for riparian vegetation dynamics: a systematic review using causal criteria analysis. *Freshwater Biology* **56**(7): 1231–1247.

Gurnell A. 2014. Plants as river system engineers. *Earth Surface Processes and Landforms* **39**(1): 4–25.

Järvelä J. 2002. Flow resistance of flexible and stiff vegetation: a flume study with natural plants. *Journal of Hydrology* **269**(1–2): 44–54.

Karrenberg S, Edwards PJ, Kollmann J. 2002. The life history of Saliaceae living in the active zone of floodplains. *Freshwater Biology* **47**(4): 733–748.

Kleinhans MG. 2010. Sorting out river channel patterns. *Progress in Physical Geography* **34**(3): 287–326.

Kleinhans MG, van den Berg JH. 2011. River channel and bar patterns explained and predicted by an empirical and a physics-based method. *Earth Surface Processes and Landforms* **36**(6): 721–738.

Kleyer M, Bekker R, Knevel I, Bakker J, Thompson K, Sonnenschein M, Poschlod P, van Groenendael J, Klimeš L, Klimešová J, Klotz S, Rusch G, Hermy M, Adriaens D, Boedeltje G, Bossuyt B, Dannemann A, Endels P, Götzenberger L, Hodgson J, Jackel AK, Kühn I, Kunzmann D, Ozinga W, Römermann C, Stadler M, Schlegelmilch J, Steendam H, Tackenberg O, Wilmann B, Cornelissen J, Eriksson O, Garnier E, Peco B. 2008. The LEDA Traitbase: a database of life-history traits of the Northwest European flora. *Journal of Ecology* **96**(6): 1266–1274.

Kui L, Stella JC, Lightbody A, Wilcox AC. 2014. Ecogeomorphic feedbacks and flood loss of riparian tree seedlings in meandering channel experiments. *Water Resources Research* **50**(12): 9366–9384.

Langendoen EJ. Evaluation of the effectiveness of selected computer models of depth-averaged free surface flow and sediment transport to predict the effects of hydraulic structures on river morphology, Technical Report, US Department of Agriculture Oxford, Mississippi, 2001.

Legionnet A, Faivre-Rampant P, Villar M, Lefevre F. 1997. Sexual and asexual reproduction in natural stands of Populus nigra. *Botanica Acta* **110**(3): 257–263.

Lesser G, Roelvink J, van Kester J, Stelling G. 2004. Development and validation of a three-dimensional morphological model. *Coastal Engineering* **51**(8–9): 883–915.

Luhar M, Nepf HM. 2013. From the blade scale to the reach scale: a characterization of aquatic vegetative drag. *Advances in Water Resources* **51**: 305–316.

Luhar M, Rominger J, Nepf H. 2008. Interaction between flow, transport and vegetation spatial structure. *Environmental Fluid Mechanics* **8**(5–6): 423–439.

Murray AB, Paola C. 2003. Modelling the effect of vegetation on channel pattern in bedload rivers. *Earth Surface Processes and Landforms* **28**(2): 131–143.

Murray AB, Knaapen MAF, Tal M, Kirwan ML. 2008. Biomorphodynamics: physical-biological feedbacks that shape landscapes. *Water Resources Research* **44**(11): 1–18.

Nicholas AP. 2013. Modelling the continuum of river channel patterns. *Earth Surface Processes and Landforms* **38**(10): 1187–1196.

Perucca E, Camporeale C, Ridolfi L. 2007. Significance of the riparian vegetation dynamics on meandering river morphodynamics. *Water Resources Research* **43**(3): 1–10.

Peters B. Successie van natuurlijke uiterwaardlandschappen [in Dutch], Technical Report , Bureau Drift and Katholieke Universiteit Nijmegen Berg en Dal, 2002.

Pollen-Bankhead N, Simon A. 2010. Hydrologic and hydraulic effects of riparian root networks on streambank stability: is mechanical root-reinforcement the whole story. *Geomorphology* **116**(3–4): 353–362.

Rinaldi M, Casagli N. 1999. Stability of streambanks formed in partially saturated soils and effects of negative pore water pressures: the Sieve River (Italy). *Geomorphology* **26**(4): 253–277.

Rivaes RP, Rodríguez-Gonzàlez PM, Ferreira MT, Pinheiro AN, Politti E, Egger G. 2014. García-Arias A, Francès F. *Modeling the evolution of riparian woodlands facing climate change in three European rivers with contrasting flow regimes. PloS one* **9**(10): 14.

Roberts A. 2003. *River Processes: An Introduction to Fluvial Dynamics*. Oxford University Press: New York.

Schuurman F, Marra WA, Kleinhans MG. 2013. Physics-based modeling of large braided sand-bed rivers: bar pattern formation, dynamics, and sensitivity. *Journal of Geophysical Research: Earth Surface* **118**(4): 2509–2527.

Schuurman F, Shimizu Y, Iwasaki T, Kleinhans M. 2015. Dynamic meandering in response to upstream perturbations and floodplain formation. *Geomorphology* (in press).

Simon A, Collison AJC. 2002. Quantifying the mechanical and hydrologic effects of riparian vegetation on streambank stability. *Earth Surface Processes and Landforms* **27**(5): 527–546.

Solari L, Oorschot MV, Belletti B, Hendriks D, Rinaldi M. 2015. Advances on modelling riparian vegetation–hydromorphology interactions. *River Research and Applications* (early view, special issue paper).

Stella JC, Battles JJ, Orr BK, McBride JR. 2006. Synchrony of seed dispersal, hydrology and local climate in a semi-arid river reach in California. *Ecosystems* **9**(7): 1200–1214.

Struiksma N. 1986. Prediction of 2D bed topography in rivers. *Journal of hydraulic Engineering* **1**(8): 1169–1182.

Tal M, Paola C. 2010. Effects of vegetation on channel morphodynamics: results and insights from laboratory experiments. *Earth Surface Processes and Landforms* **35**(9): 1014–1028.

Temmerman S, Bouma T, Van de Koppel J, Van der Wal D, De Vries M, Herman P. 2007. Vegetation causes channel erosion in a tidal landscape. *Geology* **35**(7): 631–634.

Tickner DP, Angold PG, Gurnell aM, Mountford JO. 2001. Riparian plant invasions: hydrogeomorphological control and ecological impacts. *Progress in Physical Geography* **25**(1): 22–52.

Tockner K, Stanford J. 2002. Riverine flood plains: present state and future trends. *Environmental Conservation* **29**(3): 308–330.

Van Dijk WM, Teske R, Kleinhans MG. 2013. van de Lageweg WI. *Effects of vegetation distribution on experimental river channel dynamics. Water Resources Research* **49**(11): 7558–7574.

Van Dijk WM, Schuurman F, Van de Lageweg WI, Kleinhans MG. 2014. Bifurcation instability and chute cutoff development in meandering gravel-bed rivers. *Geomorphology* **213**: 277–291.

Van Splunder I, Coops H, Voesenek L, Blom W. 1995. Establishment of alluvial forest species in floodplains: the role of dispersal timing, germination characteristics and water level fluctuations. *Acta Botanica Neerlandica* **44**(3): 269–278.

Van Velzen E, Jesse P, Cornelissen P, Coops H. Stromingsweerstand vegetatie in uiterwaarden. Deel 1 Handboek versie 1 [in Dutch], Technical Report , RIZA Arnhem, 2003a.

Van Velzen E, Jesse P, Cornelissen P, Coops H. Stromingsweerstand vegetatie in uiterwaarden. Deel 2 achtergronddocument versie 1 [in Dutch], Technical Report , RIZA Arnhem, 2003b.

Vaughan IP, Diamond M, Gurnell AM, Hall KA, Jenkins A, Milner NJ, Naylor LA, Sear DA, Woodward G, Ormerod SJ. 2009. Integrating ecology with hydromorphology: a priority for river science and management. *Aquatic Conservation: Marine and Freshwater Ecosystems* **19**(1): 113–125.

Vesipa R, Camporeale C, Ridolfi L. 2015. Noise-driven cooperative dynamics between vegetation and topography in riparian zones. *Geophysical Research Letters* **42**: 1–10.

Wolf RJ, Stortelder A, De Waal R. 2001 Ooibossen [in Dutch]. Stichting Uitgeverij van de Koninklijke Nederlandse Natuurhistorische Vereniging, Utrecht.

Zong L, Nepf H. 2011. Spatial distribution of deposition within a patch of vegetation. *Water Resources Research* **47**(3): 1–12.

Supporting Information

Movies of the three basic model simulations can be found in the online version of this article at the publisher's web site. S1: reference scenario without vegetation, S2: static vegetation scenario, S3: dynamic vegetation scenario.